Nanoindentation of NiAl and Ni_3Al crystals on (100), (110), and (111) surfaces: A molecular dynamics study

Richard Seymour,[1] Anne Hemeryck,[2,3] Ken-ichi Nomura,[1] Weiqiang Wang,[1] Rajiv K. Kalia,[1] Aiichiro Nakano,[1] and Priya Vashishta[1]
[1]*Collaboratory for Advanced Computing and Simulations, Department of Chemical Engineering & Materials Science, Department of Physics & Astronomy, Department of Computer Science, University of Southern California, Los Angeles, California 90089-0242, USA*
[2]*CNRS, LAAS, 7 avenue du Colonel Roche, F-31400 Toulouse, France*
[3]*Universite de Toulouse, LAAS, F-31400 Toulouse, France*

(Received 28 October 2013; accepted 4 February 2014; published online 7 April 2014)

Molecular dynamics simulations were performed to study the nanoindentation of NiAl and Ni_3Al crystals on three surfaces: (100), (110), and (111). The calculated load-displacement curves show discrete drops at certain indentation depths, indicating dislocation bursts during indentation. The hardness values for the two materials were found to depend significantly on the indented crystallographic plane: the (100) surface is the softest for NiAl and the hardest for Ni_3Al. We also found distinctive deformation activities in the subsurface region in Ni_3Al crystals, while dislocation loops propagate deep into the substrate in NiAl systems. © *2014 Author(s). All article content, except where otherwise noted, is licensed under a Creative Commons Attribution 3.0 Unported License.* [http://dx.doi.org/10.1063/1.4867168]

Nickel aluminide is an intermetallic compound with important technological applications because of its light weight as well as its resistance to oxidation, corrosion, structural deformation, and yield strength at high temperatures.[1–6] In intermetallic compounds, the coexistence of metallic and covalent interatomic bonding[7,8] makes their mechanical properties highly nontrivial. An example is the anomalous yield strength of Ni_3Al at elevated temperatures. Unlike ordinary materials, it exhibits maximum strength before melting, as the temperature increases. The strength of nickel aluminide also depends on crystallographic orientations. In transition metal alloys such as NiAl, structural transformation is observed under applied stress. In the molecular dynamics (MD) simulation of nanowires carried out by Park,[9] the strain response of NiAl was shown to change from brittle to super elastic via martensitic phase transformation. Zhang *et al*. suggested that in NiAl, dislocations can serve plastic accommodation during the growth of martensitic transformation.[10] Using transmission electron microscopy, Zhu *et al*. studied the orientation dependence of creep behavior in Ni_3Al single crystal and observed a crossover of slip systems—from octahedral to cubic planes—between the primary and secondary creep stages.[11] Kozlov *et al*. studied the anomalous temperature dependence of the yield point in Ni_3Al and attributed it to the anisotropic atomic arrangement in dislocation glide planes.[12] Though nickel aluminide compounds have been widely used in gas turbines and jet engines, their brittleness hinders their use as thin films in many engineering applications.[1] One approach toward overcoming this difficulty may be through nanostructural design. In fact, unique mechanical properties have been observed experimentally for Ni_3Al nanocubes[6] and through MD simulations for Ni_3Al nanowires.[13] A key to controlling these nanomechanical properties is the atomistic understanding of anisotropic mechanical responses on different crystallographic surfaces.

Nanoindentation is a widely used experimental technique to examine the mechanical response of materials, including the slip system, through localized damage induced by a sharp indenter tip.[14–18] A number of nano-to-micro indentation studies has been carried out on NiAl and Ni_3Al single crystals,[18–20] multilayered thin films,[21] NiAl-coated Ni substrate,[22] and other Ni alloys,[23] which shows an indentation size effect and anisotropic hardness with respect to the indenter orientation.[24–27] MD simulations have been used to investigate atomistic processes during nanoindentation for metals and ceramics.[28–30] Although extensive research has been done on nickel aluminide systems, a comprehensive study of their mechanical responses is still lacking. In this work, we have performed nanoindentation MD simulations on three nickel aluminide surfaces: (100), (110), and (111) for B2-NiAl and $L1_2$-Ni_3Al crystals.

Figures 1(a)–1(c) show the unit cell structure of B2 NiAl and $L1_2$ Ni_3Al crystals and a schematic of a nanoindentation simulations setup. We used an embedded atom method (EAM) type potential developed by Chen, Srolovitz, and Voter[31] to investigate the NiAl and Ni_3Al systems. With EAM's interatomic potential, Chen *et al*. studied the grain boundary (GB) structure, GB cohesive energy, and stain distribution around GBs. To perform MD simulations of NiAl systems, we also examined the cohesive energy, bulk modulus, and surface energy of B2-NiAl, which show reasonable agreement with the literature. The film dimensions for the six systems are approximately 180 Å, 180 Å, and 170 Å in the x-, y-, and z- directions, respectively. NiAl systems with the (100), (110), and (111) surfaces contain 450 560, 560 000, and 476 928 atoms. The numbers of atoms for Ni_3Al crystals with the (100), (110), and (111) surfaces are 486 720, 492 544, and 471 744, respectively. Periodic boundary conditions are applied in the x- and y- directions perpendicular to the indentation direction. The thin film is initially quenched to 0 K to relax the surfaces and is gradually heated up and thermalized at 300 K. A thin layer of atoms, 5 Å from the bottom of the film in the z- direction, is fixed to hold the film during simulation. In all simulations, we use a

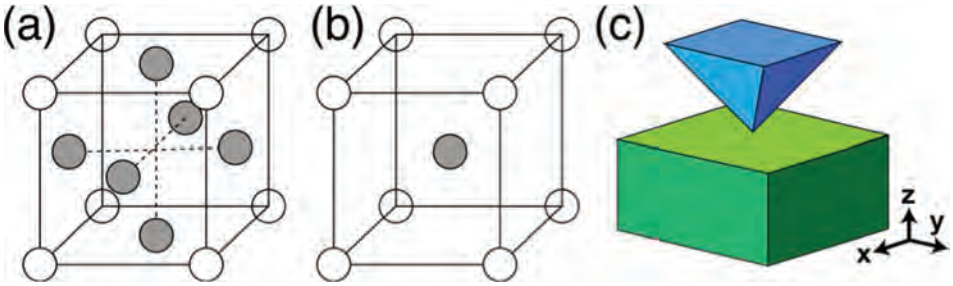

FIG. 1. (a) B2 NiAl crystalline unit cell and (b) $L1_2$ Ni_3Al crystalline unit cell, where gray and white circles represent Ni and Al atoms, respectively. (c) Schematic of nanoindentation simulation setup. Blue pyramidal shape and the green rectangle represent an indenter and a substrate, respectively.

four-faced pyramidal-shape rigid indenter with a 90° edge angle cut out of an fcc crystal. The indenter atoms interact with film atoms through pure repulsion. One MD time step is 2.5 fs throughout the simulations. During the loading phase, the indenter is moved into the film by 0.5 Å for 1000 time steps. Subsequently, we relax the system by holding the indenter for 9000 time steps. We repeat this process until the total indentation depth reaches approximately one-quarter of the film thickness, corresponding to 40 Å from top surface. During unloading phase, we use the same schedule except for reversing the direction of the indenter displacement. To indentify defect atoms, we used coordination number and common neighborhood parameter (CNP).[32]

Table I summarizes hardness values (i.e., the indenter load divided by the projected indentation area) obtained for the six simulations. In the NiAl systems, the (100) surface is notably softer than the (110) and (111) surfaces. On the other hand, the (100) surface is harder than the other two surfaces in the Ni_3Al systems.

Figure 2 shows the load-displacement curves (*P-h*) and hardness for the NiAl (100) and Ni_3Al (100) systems. We observe several drops in the *P-h* curves during the loading phase (pop in) indicating discrete deformation events in our systems. The hardness values of the six systems exhibit the indentation size effect and crystallographic-orientation dependency.

Figure 3 below shows snapshots of the dislocation activities in NiAl (100) at the indentation depth $h = 40$ Å. During indentation, dislocations form a loop structure (pointed by the yellow arrow), which glides in the $[\bar{1}00]$ direction moving away from the indenter. The loop develops into a skewed square shape[33] with the sides oriented towards the $[\bar{1}\bar{1}2]$ and $[\bar{1}12]$ directions (see Fig. 3(b)). At $h = 40$ Å, we also observe the nucleation of second dislocation loop (pointed by the red arrow).

Figure 4 shows the dislocation loop under the indenter with half of the top surface of the system cut away on the (011) plane. In the NiAl (110) and NiAl (111) simulations, two dislocation loops are formed one after the other, parallel to each other and separated by about 15 Å.[34] In contrast to the NiAl systems, dislocation activities are rather confined within the subsurface regions in the Ni_3Al crystals. Figure

TABLE I. Hardness of NiAl and Ni_3Al with the (100), (110), and (111) surfaces.

Hardness (GPa)	(100)	(110)	(111)
NiAl	11.9	16.9	17.0
Ni_3Al	21.5	17.8	18.4

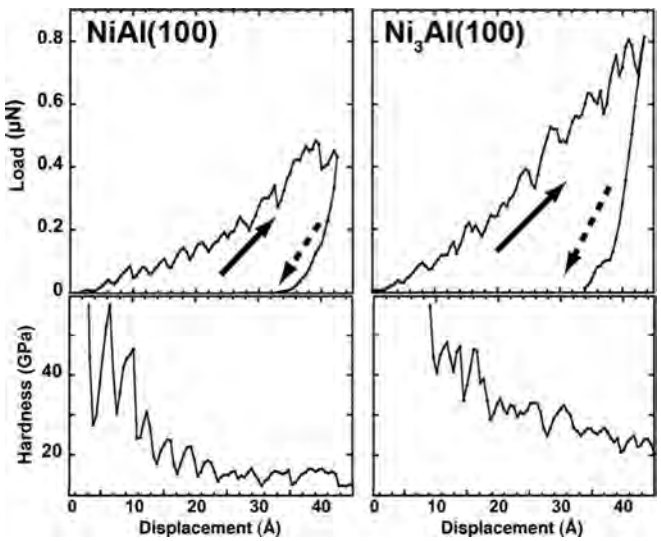

FIG. 2. (Left) Load-displacement curve and hardness of NiAl with the (100) surface. Solid and dashed arrows indicate the loading and unloading processes, respectively. (Right) Load-displacement curve and hardness of Ni_3Al with the (100) surfaces.

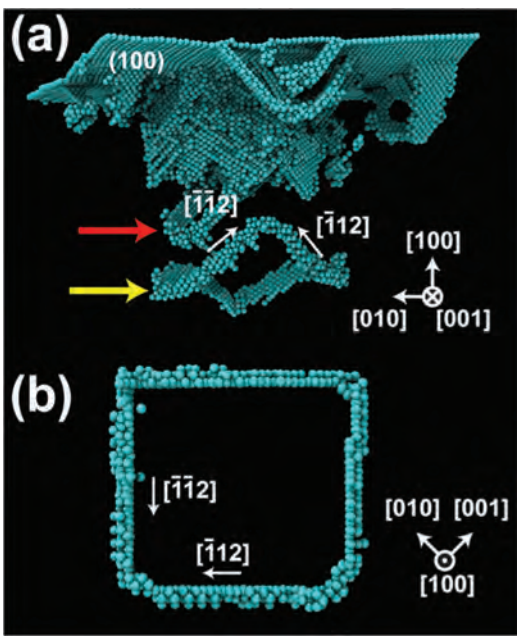

FIG. 3. (a) Snapshot of dislocation activity in NiAl (100) at indentation depth $h = 40$ Å. Defect atoms detected by coordination number are shown. The red arrow indicates a new dislocation loop that begins to form. (b) Top-view of the "square-shape" dislocation loop (pointed by the yellow arrow in (a)) projected on the (100) plane.

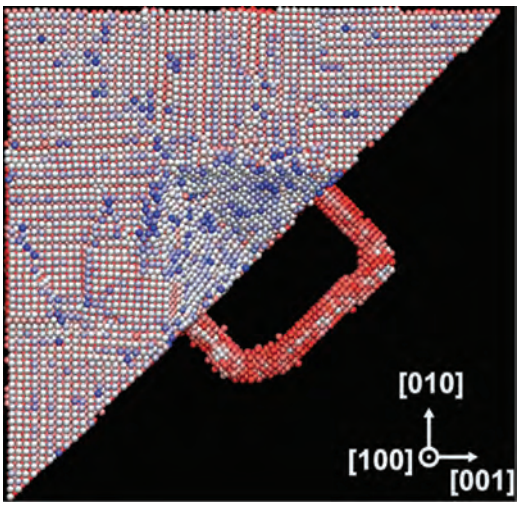

FIG. 4. The dislocation loop underneath the indenter in the NiAl (100) system. For clarity, indenter atoms are not shown. The defect atoms are indentified by their coordination number and colored by the common neighborhood parameter value.

5(a) displays a snapshot of dislocation activities near the indenter at the indentation depth $h = 25$ Å. By increasing indentation depth, dislocations nucleate from the corner of the indenter and develop into a V-shape that subsequently travels away from the indenter via edge dislocations on the {111} family of planes. Figure 5(b) shows the distribution of surface atoms in the vicinity of the V-shape slip planes

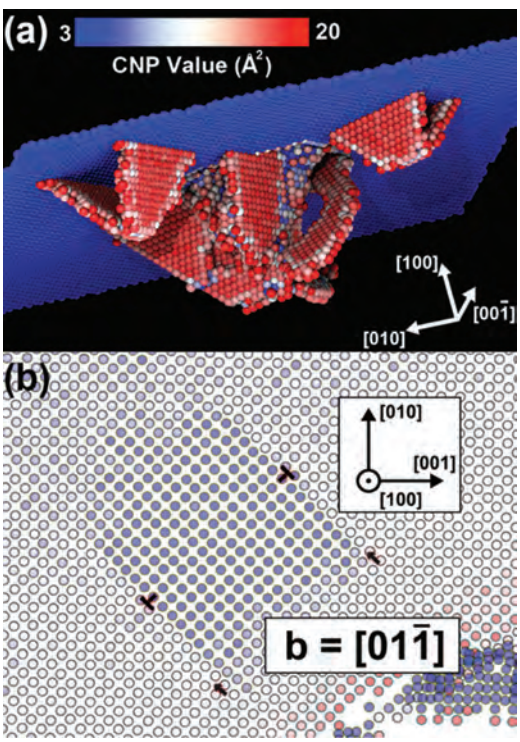

FIG. 5. (a) Nucleation and propagation of V-shape {111} slip planes in Ni_3Al (100) at indentation depth $h = 25$ Å. Atoms are color-coded by the common neighborhood parameter values. Atoms in the indenter and in the bulk condition are not shown for clarity. (b) Top view of the surface atoms configuration around the V-shape slip planes in Ni_3Al (100). Circles show the position of the surface atoms that are color-coded by their relative coordinates in [100]. The T-marks indicate the position of the dislocations. The indenter is at right-bottom corner and not shown for clarity.

looking down on the (100) plane. Burgers vector analysis shows that the two partial dislocations, $\frac{1}{6}\langle 11\bar{2}\rangle$ and $\frac{1}{6}\langle \bar{1}2\bar{1}\rangle$, comprise the V-shape dislocations. This partial dislocation accounts for the 1.1 Å height difference of the atoms within the V-shape region compared to outside.

In summary, we performed MD simulations of nanoindentation on NiAl and Ni_3Al crystals with the (100), (110), and (111) surfaces. Discrete drops in the obtained *P-h* curves were found to arise from dislocation bursts underneath the indenter. The hardness of the NiAl and Ni_3Al system shows significant dependence on the crystallographic planes, specifically the lowest hardness for NiAl (100) and the greatest value for Ni_3Al (100). Our MD simulations have revealed that plastic activities are confined near the subsurface region close to the indenter in the case of Ni_3Al systems while dislocation loops propagate into the substrate in the NiAl systems.

This research was initially supported by the Defense Threat Reduction Agency (DTRA), Grant No. HDTRA1-08-1-0036 and has been completed with the support from the Office of Naval Research (ONR), Air Warfare and Weapons Department, grant No. N00014-12-1-0555. Authors would like to thank Dr. Suhithi Peiris and Dr. Clifford Bedford for their encouragement and continued support for this research project. Computations were performed at the University of Southern California High Performance Computing Center using the 560 teraflops Linux cluster and the 4,096-processor Linux cluster at the Collaboratory for Advanced Computing and Simulations.

[1]C. T. Liu and J. O. Stiegler, Science **226**(4675), 636–642 (1984).
[2]R. Darolia, J. Mater. Sci. Technol. **10**, 157 (1994).
[3]S. C. Deevi and V. K. Sikka, Intermetallics **4**(5), 357–375 (1996).
[4]V. K. Sikka, S. C. Deevi, S. Viswanathan, R. W. Swindeman, and M. L. Santella, Intermetallics **8**(9-11), 1329–1337 (2000).
[5]E. N. Kablov, B. S. Lomberg, V. P. Buntushkin, E. P. Golubovskii, and S. A. Muboyadzhyan, Met. Sci. Heat Treat. **44**(7-8), 284–287 (2002).
[6]R. Maass, L. Meza, B. Gan, S. Tin, and J. R. Greer, Small **8**(12), 1869–1875 (2012).
[7]A. G. Fox and M. A. Tabbernor, Acta Metall. Mater. **39**(4), 669–678 (1991).
[8]Z. W. Lu, S. H. Wei, and A. Zunger, Acta Metall. Mater. **40**(9), 2155–2165 (1992).
[9]H. S. Park, Nano Lett. **6**(5), 958–962 (2006).
[10]X. M. Zhang, B. Li, X. W. Sha, Z. Q. Sun, and R. Li, J. Mater. Sci. Technol. **16**(4), 370–374 (2000).
[11]W. H. Zhu, D. Fort, I. P. Jones, and R. E. Smallman, Acta Mater. **46**(11), 3873–3881 (1998).
[12]E. V. Kozlov, Y. A. Abzaev, Y. V. Solov'eva, V. A. Starenchenko, and N. A. Koneva, Bull. Russ. Acad. Sci.: Phys. **73**, 1022 (2009).
[13]Y. J. Wang, G. J. J. Gao, and S. Ogata, Appl. Phys. Lett. **102**(4), 041902 (2013).
[14]D. Saraev and R. E. Miller, Modell. Simul. Mater. Sci. Eng. **13**(7), 1089–1099 (2005).
[15]C. A. Schuh, J. K. Mason, and A. C. Lund, Nat. Mater. **4**(8), 617–621 (2005).
[16]A. H. W. Ngan and P. C. Wo, Philos. Mag. **86**(9), 1287–1304 (2006).
[17]Y. L. Chiu and A. H. W. Ngan, Acta Mater. **50**(10), 2677–2691 (2002).
[18]W. Wang and K. Lu, J. Mater. Res. **17**(9), 2314–2320 (2002).
[19]M. L. Weaver, M. E. Stevenson, and R. C. Bradt, Mater. Sci. Eng., A **345**(1-2), 113–117 (2003).
[20]F. Ebrahimi, A. Gomez, and T. G. Hicks, Scr. Mater. **34**(2), 337–342 (1996).
[21]X. K. Meng, H. Vehoff, and A. H. W. Ngan, J. Mater. Res. **15**(12), 2595–2597 (2000).

[22]B. Ning, M. E. Stevenson, M. L. Weaver, and R. C. Bradt, Surf. Coat. Technol. **163**, 112–117 (2003).
[23]F. W. Herbert, B. Yildiz, and K. J. Van Vliet, "Nanoindentation induced deformation near grain boundaries of corrosion resistant nickel alloys," (Mater. Res. Soc. Symp. Proc., 2011), Vol. 1297, pp. 187–192.
[24]W. Wang, C. B. Jiang, and K. Lu, Acta Mater. **51**(20), 6169–6180 (2003).
[25]S. Shim, H. Bei, E. P. George, and G. M. Pharr, Scr. Mater. **59**(10), 1095–1098 (2008).
[26]P. C. Wo, L. Zuo, and A. H. W. Ngan, J. Mater. Res. **20**(2), 489–495 (2005).
[27]J. Li, K. J. Van Vliet, T. Zhu, S. Yip, and S. Suresh, Nature **418**(6895), 307–310 (2002).
[28]P. Walsh, R. K. Kalia, A. Nakano, P. Vashishta, and S. Saini, Appl. Phys. Lett. **77**(26), 4332–4334 (2000).
[29]I. Szlufarska, A. Nakano, and P. Vashishta, Science **309**(5736), 911–914 (2005).
[30]V. Yamakov, D. Wolf, S. R. Phillpot, A. K. Mukherjee, and H. Gleiter, Nat. Mater. **1**(1), 45–48 (2002).
[31]S. P. Chen, D. J. Srolovitz, and A. F. Voter, J. Mater. Res. **4**(1), 62–77 (1989).
[32]H. Tsuzuki, P. S. Branicio, and J. P. Rino, Comput. Phys. Commun. **177**(6), 518–523 (2007).
[33]J. D. Honeycutt and H. C. Andersen, J. Phys. Chem. **91**(19), 4950–4963 (1987).
[34]T. C. Tisone, G. W. Marshall, and J. O. Brittain, J. Appl. Phys. **39**(8), 3714–3717 (1968).